Design Optimization of Multi-Input Reconfigurable Capacitive DC-DC Converters: A CAD Tool Approach

Abdelrahman Elabany
EECE Department,
Cairo University, Giza, Egypt
abdelrahman.elabany@gmail.com

Amin Nassar
EECE Department,
Cairo University, Giza, Egypt

Hassan Mostafa
Cairo University, Giza, Egypt
University of Science and technology, Nanotechnology and Nanoelectronics Program , Zewail City of Science and Technology, October Gardens, 6th of October, Giza 12578, Egypt.
hmostafa@uwaterloo.ca

2021 IEEE International Symposium on Circuits and Systems (ISCAS) | 978-1-7281-9201-7/20/$31.00 ©2021 IEEE | DOI: 10.1109/ISCAS51556.2021.9401710

***Abstract*— Energy harvesting from multiple sources is a more robust method for powering Internet of Things (IoT) nodes and similar wireless systems compared to harvesting from a single source. This work provides a description of an optimization CAD tool for reconfigurable capacitive DC-DC converters with multiple inputs used for energy-harvesting from multiple sources with varying levels of input power. The tool estimates the theoretical maximum efficiency for each converter configuration, along with the input power condition that achieves this performance. In addition, for given values of the available power from the harvesting sources connected to the DC-DC converter inputs, the proposed CAD tool finds the best converter configuration for that power state of the harvesters.**

Keywords—energy-harvesting, DC-DC conversion, power conversion efficiency optimization, CAD tool

I. INTRODUCTION

Energy harvesting is an attractive way to power wireless systems, such as IoT applications and implantable and wearable devices. Multiple-input energy harvesters are suitable for such systems; where different sources such as solar, thermal, Piezoelectric, and RF energy sources are cultivated as the availability of each power source varies with time, thus providing a more robust operation [1], [2].

Fully integrated capacitive DC-DC converters have a major advantage over inductive DC-DC converters which have traditionally been used in power management systems, as they lack the bulky external inductor [3]. However, a major disadvantage of capacitive converters is the constant voltage conversion ratio (VCR) of each configuration, which causes drop in efficiency with the deviation of the operation point.

For some applications, the single-input single-output (SISO) converter has a VCR value that remains relatively constant during operation. This makes the design space for the converter relatively limited. Modulating the output resistance (through, for example, varying the switching frequency [4]) may be enough to maintain an acceptable power conversion efficiency (PCE) across operation. For a SISO converter used for energy harvesting, the available power from the source varies a lot across time, and thus creating the need for having a reconfigurable converter [5]. The design space in this case is still fairly limited, since the input harvester power range can be divided into a reasonable number of states with separate design requirements (for example, low, medium, and high input power states).

However, having multiple energy harvesting sources makes the design less straight-forward [6], since the design space becomes large fairly quickly, as illustrated in Fig. 1. Thus, there is a need for tools to analyze the performance of the capacitive DC-DC converters with multiple inputs and reconfigurable internal connections. This work provides this optimization CAD tool.

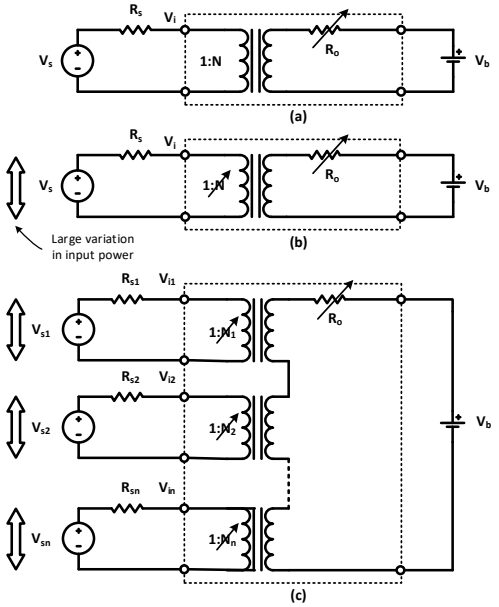

Fig. 1 Comparison of (a) a SISO converter with a relatively constant input. (b) a SISO converter connected to a harvesting source, and (c) a MISO converter connected to multiple harvesting sources. Varying control parameters are denoted by arrows.

To the best of the authors' knowledge, this is the first attempt to develop this kind of automation for multi-input capacitive converter design.

This paper is organized as follows: Section II gives a detailed description of the optimization method used by the CAD tool. Simulation results are given in Section III. Finally, the whole work is concluded in Section IV.

II. OPTIMIZATION TOOL DESCRIPTION

A. Overview

The purpose of the developed optimization tool is to facilitate the design of a reconfigurable capacitive DC-DC converter used for energy harvesting from multiple sources. It achieves this through the following:

1. Calculating the theoretical maximum PCE that can be achieved by each converter configuration and the corresponding power state of the harvesting sources. The tool also calculates the optimum switching frequency required to achieve this performance.

978-1-7281-9201-7/21/$31.00 ©2021 IEEE

2. With reference to a simplified converter model, finding the characterizing parameters of that model that only depend on the configuration.
3. For a given set of energy harvesting sources with known available powers, finding the best converter configuration by comparing their performance using the calculated model parameters.
4. The last point can be repeated in order to provide the best configuration for different input power states.

Fig. 2 shows a simplified flowchart illustrating the tool operation. The tool was developed using LabVIEW. The different steps are explained in the following sub-section.

B. Method

1) Generating a list of possible configurations

Given the maximum number of stages and the number of input sources, the tool generates a list of possible DC-DC configurations.

Each configuration is defined by three groups of parameters that determine the connectivity of the converter as shown in Fig. 3:

- The first input of the first stage (V_{a1})
- The second input of all stages (V_{b1} to V_{bNstg})
- The gate switching voltage of each stage (V_{sw1} to V_{swNstg})

2) Characterizing each configuration

The simplified model illustrated in Fig. 4 is characterized by the following parameters for each configuration:

a) The array N_v: defined as the voltage gain from each of the converter inputs to the converter output assuming no losses. This number is also equal to the current drawn from each input port divided by the output current assuming no losses. The dependent voltage and current source represenation of Fig. 4 is equivalent to the common ideal transformer representation of Fig. 1.

b) The parameter $A_{GRo} \equiv G_{Ro}/G_f$: represents the output series conductance value normalized with respect to the conductance of the flying capacitance used ($G_f = 2\pi f C_f$). This represents the Charge Redistribution Loss (CRL). A similar method of modeling CRL is used in earlier works, such as in [5] and [7].

c) The parameter $A_{Gpo} \equiv G_{po}/G_f$: represents the output parallel conductance value normalized with respect to the conductance of the flying capacitance used. This represents the total parasitic switching losses (top plate, bottom plate and gate switching).

A similar method of modeling switching losses is used in earlier works, such as in [8] and [9] where it is modelled as a shunt resistance at the output of the ideal transformer, and in [1] where the resistance is placed at the input of the ideal transformer. In this work, the loss is lumped at the output of the converter, since it represents the node with the least variation, and thus choosing to model the loss at this point provides more accurate modelling for varying input voltages.

This parameter is calculated by estimating the effective normalized value of parasitic capacitances driven by each node of the system, using the simplified stage models shown in Fig. 5 and Fig. 6. These losses are referred to the output of the converter forming the total shunt resistance at that node.

For example, the power dissipated for switching the top plate capacitance per stage is:

$$p_{top} = 2 \times v_o \times (v_o - v_a) \times g_{top} \quad (1)$$

where the parameter g_{top} represents the normalization factor:

$$g_{top} = 2\pi f C_{top} = 2\pi f \alpha_{top} C_f \quad (2)$$

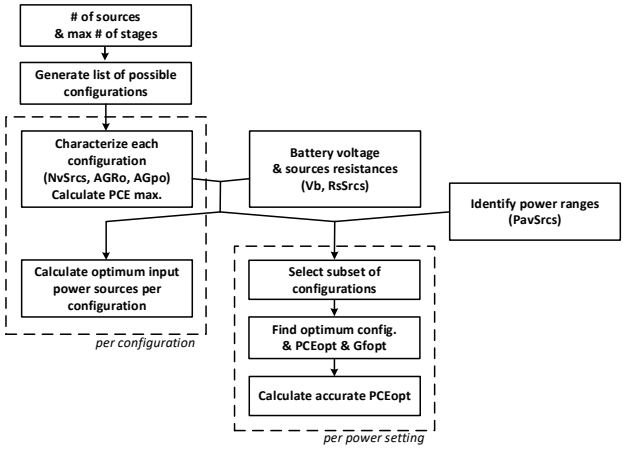

Fig. 2 Optimization tool operation flowchart

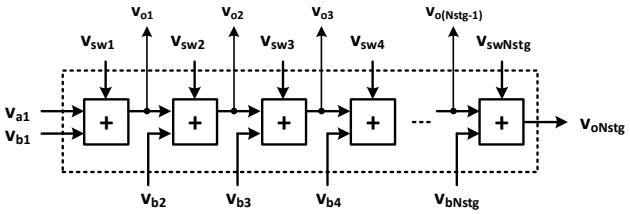

Fig. 3 Reconfigurable DC-DC converter core

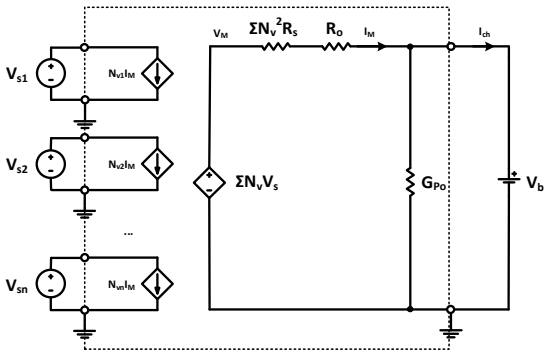

Fig. 4 Simplified converter model

Assuming no losses ($v_o \approx v_a + v_b$):

$$p_{top} \approx v_o^2 \times \left(\frac{2}{\frac{v_a}{v_b} + 1} \right) \times g_{top} \quad (3)$$

Thus, $2/(v_a/v_b + 1)$ is the effective normalized value of top plate parasitic capacitances driven by the stage output.

Similar analysis can be done for the bottom-plate and gate-switching losses. The effective normalized values of the parasitic capacitances introduced by any stage are summarized in TABLE I.

d) The maximum achievable PCE for each configuration:

The optimum operating point can be found as follows:

$$P_{ch} = \frac{\sum N_v V_s - \left(1 + G_p(R_o + \sum N_v^2 R_s)\right) V_b}{R_o + \sum N_v^2 R_s} \times V_b \quad (4)$$

$$\frac{\partial P_{ch}}{\partial G_f} = 0 \rightarrow G_{fopt} = \frac{1}{A_{GRo} \times \sum N_v^2 R_s} \times \left(\sqrt{\frac{a_V}{a_G}} - 1 \right) \quad (5)$$

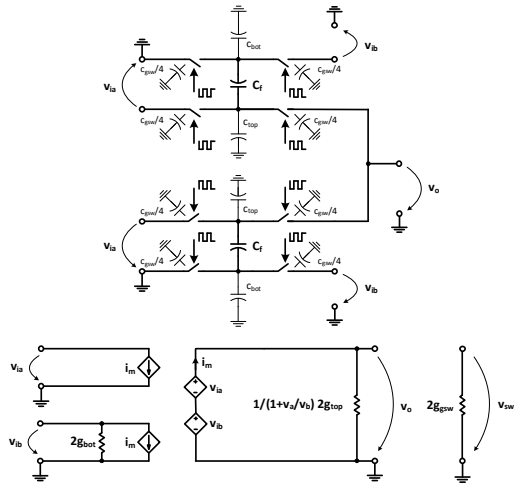

Fig. 5 Stage-model of the DC-DC converter when switched using voltage external to the stage (e.g. battery voltage)

TABLE I. STAGE PARASITIC CAP. ESTIMATE VALUES

Parasitic cap.	Normalized value	Norm. param.	Connection point
Top-plate	$2/\left(\frac{v_a}{v_b}+1\right)$	$\alpha_{top}C_f$	Stage output
Bottom-plate	2	$\alpha_{bot}C_f$	Stage input 'b'
Ext.-voltage gate-switching	2	$\alpha_{gsw}C_f$	Converter output
Cross-coupled gate-switching	1	$\alpha_{gsw}C_f$	Converter output
	$1/\left(\frac{v_a}{v_b}+1\right)$	$\alpha_{gsw}C_f$	Stage input 'b'

$$PCE_{@Gfopt} = \frac{1 - \sqrt{\frac{a_G}{a_V}}}{1 + \sqrt{a_G a_V}} \quad (6)$$

where the ratio $a_G \equiv A_{Gpo}/A_{GRo}$ represents the ratio between the switching and charge-redistribution losses, and the parameter $a_V \equiv \sum N_v V_s / V_b - 1$ describes the relationship between the input sources and the battery voltage.

- The conversion efficiency at optimum operating point ($PCE_{@Gfopt}$) reaches the maximum value for each configuration at the following condition:

$$a_{Vopt} = 2a_G + 1 + 2\sqrt{a_G(a_G + 1)} \quad (7)$$

$$\therefore PCE_{max} = \frac{1 - \sqrt{\frac{a_G}{a_{Vopt}}}}{1 + \sqrt{a_G a_{Vopt}}} \quad (8)$$

which is a function only of the converter losses for the given configuration, and not a function of the input or the output voltages. This number represents the theoretical maximum PCE achievable by the configuration.

3) Finding the optimum input power from each source per configuration

For a given set of input sources, each source can be modelled as a voltage source with a known source resistance. Given the values of these resistances, the tool finds the power state for each input source at which this maximum PCE is achieved.

$$V_{sopt} = 2 \times I_{iopt} R_s \quad (9)$$

$$V_{sopt} = 2N_v R_s \left(a_{Vopt} - \sqrt{a_G a_{Vopt}}\right) \times \frac{V_b}{\sum N_v^2 R_s} \quad (10)$$

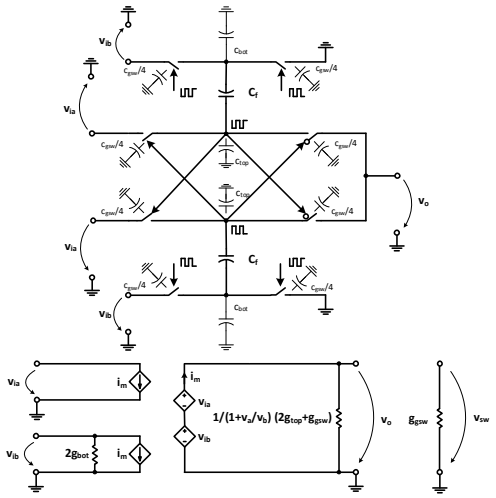

Fig. 6 Stage-model of the DC-DC converter when switched through cross-coupled configuration

4) Finding optimum configuration per input power state

The tool provides another output depending on the user-provided input power states. It selects only a favorable set of DC-DC configurations for the given input source values. The relation to be satisfied for best matching between the sources and the converter is:

$$N_{vopt} = \frac{I_{iopt}}{I_M} \quad (11)$$

For a lossless converter

$$\sum N_{vopt} V_{iopt} \approx V_b \quad (12)$$

Solving (11) and (12):

$$\therefore N_{vopt} \approx \sqrt{\frac{P_{av}}{R_s}} \times \frac{V_b}{\sum P_{av}} \quad (13)$$

This value is only a function of the harvesting sources and the battery voltage, and not a function of the configuration itself.

By selecting only converters with N_v array values close to the values found using the calculation N_{vopt} for the given set of power sources, the number of compared configurations is limited to only a subset with expected good matching with the given source powers. A user controlled variable determines the maximum allowed deviation from N_{vopt} for any input. This variable provides a compromise between runtime and coverage.

For each source setting, the PCE is then calculated for each of these selected configurations using the model parameters calculated in Section I-B-2, in order to find the optimum configuration.

5) Finding a more accurate estimate for the PCE per input power state

After finding the optimum configuration, a more accurate value for PCE is calculated using an iterative method. The required sizing of the switches is also estimated.

III. Simulation Results

The simulation setup has been established following the design parameters in TABLE II.

TABLE II. Simulation conditions

Parameter	Symbol	Unit	Value
Maximum number of stages	N_{stgmax}	_	6
Flying capacitor value	C_f	pF	10, 100
# of harvesting sources	N_{scrs}	_	3
Harvester source resistances	R_s	$k\Omega$	5, 10, 20
# of power states per harvester	N_{pwr}	_	5
Harvester available power state values	P_{av}	dBm	-40, -30, -20, 10, 0
Parasitic capacitance loss			
• Top-plate losses	$\alpha_{top} \equiv C_{top}/C_f$	%	0.1%
• Bottom-plate losses	$\alpha_{bot} \equiv C_{bot}/C_f$	%	1%
Switch characteristics			
• Characteristic res.	R_{cc}	$m\Omega.m.V$	60
• Characteristic cap.	C_{cc}	nF/m	13
• Minimum width	w_{min}	μm	3

The number of power states in this example is $(N_{srcs})^{N_{pwr}} = 125$. For each power state, the number of available configurations is 4248. The optimum configuration is selected by the tool and the PCE is estimated using the simplified model described in Section II-B-2. This provides 125 different selected configurations. Cadence PSS simulation is used in each case to find the reference value of the PCE for each of these configurations. The PCE calculated using the simple model (Fast Calc.) and the accurate recalculation described in Section II-B-5 are plotted in Fig. 7. and Fig. 8 for two different values of the flying capacitor setting.

TABLE III. shows the characterization runtime when varying different inputs to the tool such as the number of sources and the maximum number of stages. The output in this case is a list of configurations, each with the characteristic maximum efficiency, the corresponding optimum power input state, and the simplified model parameters. TABLE IV. shows the overall runtime when varying different conditions where the tool is used for finding the optimum configuration for each of the power state combinations. The time required to run a single PSS simulation for a 6 stage converter is around 60 seconds showing a clear advantage for the developed tool in estimating performance of a large number of configurations.

TABLE III. Runtime of the tool for Generating and Characterizing Configurations

# sources	max # stages	# config.	characterization time (s)	time / config. (ms)
2	6	1248	0.5	0.4
2	8	13832	3.4	0.25
5	8	333630	458	1.37

TABLE IV. Overall Runtime of the tool

# sources	max # stages	# power states / source	# config.	# power state combinations	total time (s)	time / state (ms)
2	6	5	1248	25	15.1	600
3	7	5	14580	125	57.5	460
4	6	5	14580	625	261	420

IV. Conclusions

This work has provided a novel attempt at automating capacitive multi-input DC-DC converter design used for energy harvesting. The tool described provides a fast method of characterizing the different DC-DC converter configurations and evaluating the theoretical maximum PCE of each configuration.

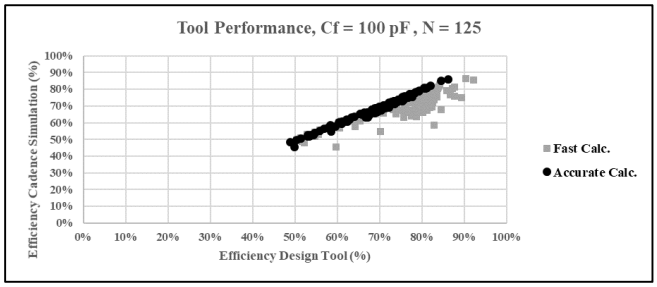

Fig. 7 Tool estimated PCE vs. PSS simulated PCE at $C_f = 100\ pF$

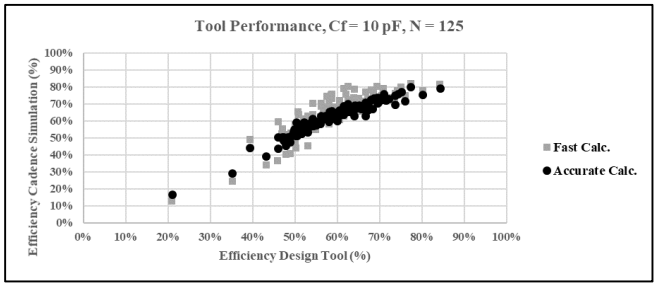

Fig. 8 Tool estimated PCE vs. PSS simulated PCE at $C_f = 10\ pF$

The tool also facilitates selecting the best configuration to use given the input power at the converter inputs. The maximum error in PCE calculation by the tool is ~ 10% with an average value of ~ 2%.

References

[1] Abouzied, Mohamed A., Hatem Osman, Vaibhav Vaidya, Krishnan Ravichandran, and Edgar Sánchez-Sinencio. "An integrated concurrent multiple-input self-startup energy harvesting capacitive-based DC adder combiner." IEEE Transactions on Industrial Electronics 65, no. 8 (2017): 6281-6290.

[2] Bandyopadhyay, Saurav, and Anantha P. Chandrakasan. "Platform architecture for solar, thermal, and vibration energy combining with MPPT and single inductor." IEEE Journal of Solid-State Circuits 47, no. 9 (2012): 2199-2215.

[3] Jung, Wanyeong, et al. "An ultra-low power fully integrated energy harvester based on self-oscillating switched-capacitor voltage doubler." IEEE Journal of Solid-State Circuits 49.12 (2014): 2800-2811.

[4] Peter, Pradeep K., and Vivek Agarwal. "On the input resistance of a reconfigurable switched capacitor DC–DC converter-based maximum power point tracker of a photovoltaic source." IEEE Transactions on power electronics 27, no. 12 (2012): 4880-4893.

[5] Villar-Pique, Gerard, Henk Jan Bergveld, and Eduard Alarcon. "Survey and benchmark of fully integrated switching power converters: Switched-capacitor versus inductive approach." IEEE Transactions on Power Electronics 28, no. 9 (2013): 4156-4167.

[6] Liu, Xiaosen, Lilly Huang, Krishnan Ravichandran, and Edgar Sánchez-Sinencio. "A highly efficient reconfigurable charge pump energy harvester with wide harvesting range and two-dimensional MPPT for Internet of Things." IEEE Journal of Solid-State Circuits 51, no. 5 (2016): 1302-1312.

[7] Seeman, Michael D., and Seth R. Sanders. "Analysis and optimization of switched-capacitor DC–DC converters." IEEE transactions on power electronics 23, no. 2 (2008): 841-851.

[8] Meyvaert, Hans, Tom Van Breussegem, and Michiel Steyaert. "A 1.65 W fully integrated 90nm bulk CMOS intrinsic charge recycling capacitive DC-DC converter: Design & techniques for high power density." IEEE Energy Conversion Congress and Exposition (2011): 3234-3241.

[9] Le, Hanh-Phuc, Seth R. Sanders, and Elad Alon. "Design techniques for fully integrated switched-capacitor DC-DC converters." IEEE Journal of Solid-State Circuits 46, no. 9 (2011): 2120-2131.